Solar turbulence in earth's global and regional temperature anomalies

Nicola Scafetta,[1,2] Paolo Grigolini,[3,4,5] Timothy Imholt,[3] Jim Roberts,[3] and Bruce J. West[1,2,6]
[1]*Physics Department, Duke University, Durham, North Carolina 27708, USA*
[2]*Electrical Engineering Department, Duke University, P. O. Box 90291, Durham, North Carolina 27708, USA*
[3]*Center for Nonlinear Science, University of North Texas, P. O. Box 311427, Denton, Texas 76203-1427, USA*
[4]*Dipartimento di Fisica dell'Università di Pisa and INFM, Via Buonarroti 2, 56127 Pisa, Italy*
[5]*Istituto dei Processi Chimico Fisici del CNR Area della Ricerca di Pisa, Via G. Moruzzi 1, 56124, Pisa, Italy*
[6]*Mathematics Division, Army Research Office, Research Triangle Park, North Carolina 27709, USA*
(Received 14 March 2003; published 26 February 2004)

This paper presents a study of the influence of solar activity on the earth's temperature. In particular, we focus on the repercussion of the fluctuations of the solar irradiance on the temperature of the Northern and Southern hemispheres as well as on land and ocean regions. While solar irradiance data are not directly analyzed, we make use of a published solar irradiance reconstruction for long-time-scale fluctuations, and for short-time-scale fluctuations we hypothesize that solar irradiance and solar flare intermittency are coupled in such a way that the solar flare frequency fluctuations are stochastically equivalent to those of the solar irradiance. The analysis is based upon wavelet multiresolution techniques and scaling analysis methods for processing time series. The limitations of the correlation analysis applied to the short-time-scale fluctuations are discussed. The scaling analysis uses both the standard deviation and the entropy of the diffusion generated by the temperature signals. The joint use of these two scaling methods yields evidence of a Lévy component in the temporal persistence of the temperature fluctuations within the temporal range from a few weeks to a few years. This apparent Lévy persistence of the temperature fluctuations is found, by using an appropriate model, to be equivalent to the Lévy scaling of the solar flare intermittency. The mean monthly temperature data sets cover the period from 1856 to 2002.

DOI: 10.1103/PhysRevE.69.026303 PACS number(s): 47.27.Nz, 95.75.Wx, 05.40.Fb, 05.45.Tp

I. INTRODUCTION

A dominant characteristic of meteorological data is extreme variability. The same is true of average global quantities such as temperature. Monin [1] discussed this broadband response that makes the predictability of weather patterns from deterministic primitive equations so uncertain. The physics of weather is described by the coupling of nonlinear hydrodynamic equations of the oceans and atmosphere to the nonequilibrium thermodynamic equations for energy, mass density, and heat transport, together with the appropriate boundary conditions and initial values for the field variables. Finally, there is the external driving of these processes by the total solar irradiance (TSI). Even the simplest model of these nonlinear processes was shown by Lorenz [2] to have nonperiodic, that is, chaotic, solutions. Herein we are not interested in the weather, except insofar as short-time measurements of meteorological variables can provide a data base from which to determine longer-time effects, such as the variability in climate.

Weather is made up of the local, short-time, variations in wind, temperature, and precipitation patterns. Climate, on the other hand, consists of large-scale, long-time, variations in these same meteorological patterns. Therefore, it should be possible, in principle, to average the equations of motion for weather, across sufficiently large space and time scales, to obtain the equations of motion for climate. Lindenberg and West [3], using such a coarse-graining procedure, provided the first systematic derivation of stochastic mode rate equations for a geophysical hydrodynamic system, starting from the deterministic primitive equations. Based on these early results, we anticipate that the theoretical dynamical equations for climate are stochastic, nonlinear, and contain memory effects. However, we do not undertake the daunting task of deriving these equations here, but rather we examine coarse-grained data sets of global temperature and from these analyses deduce these same characteristics of climate variation.

It might appear from the above considerations that the least dynamic of the factors influencing weather and climate is the irradiance from the sun, but nothing could be farther from the truth. The historical recognition that the sun warms the earth has suggested a direct connection between global temperature and solar activity. However, it is also known that the earth's temperature is characterized by many factors, affecting one another as heat is transferred across different regions of the earth [4]. It was established in the first quarter of the last century by Sir Gilbert Walker [5] that the world's weather is strongly influenced by the variability of the solar activity. For example, Sir Gilbert determined that solar activity affects large-scale pressure differences on the earth's surface and thereby modifies patterns of rainfall. It was established about the same time, circa 1926 [6], that global rainfall maxima coincide with maxima of sunspot activity. Brooks [6] also gave the variations in solar activity based on sunspot number historical records as one of the major causes of climate change on the time scale of a few hundred years.

Today, global climate change is analyzed with tools developed within the science of complexity, for example, the Kolmogorov-Sinai entropy is used as a quantitative measure of uncertainty in nonlinear dynamical systems with chaotic solutions [7,8]. We apply some of these nonlinear techniques

herein to establish that, because the radiation from the sun warms the earth, any observable changes in the intensity of TSI induce changes in the earth's global temperature. We support this hypothesis by analyzing both long- and short-time-scale affinity between solar activity and temperature fluctuations.

Long-time-scale affinity is measured via a correlation wavelet multiresolution analysis. In particular, the rise in the average temperature of the earth over the past century is found to track the increases in solar activity estimated with a TSI reconstruction by Lean *et al.* [9] based on sunspot number historical records over the same time period, in a statistically significant way. Short-time-scale affinity, which is not detected by the cross-correlation analysis, is ascertained by studying the statistics of solar flare activity which has a non-Gaussian, that is, Lévy nature that is found to be equivalent to the statistics of the variations in the global temperature over the past 140 years. We emphasize that the literature on the influence of solar activity on the earth's climate for the long time scale is very large (see, for example, some recent articles [10,11]) but for the short time scale such evidence is not as direct.

The complexity of hydrodynamic turbulence in the earth's oceans and atmosphere is exceeded only by the hydromagnetic turbulence at the surface of the sun. The nonlinear dynamics of the sun's plasma may well account for the fact that science is unable to predict the number of sunspots and the occurrence of solar flares as a function of time even though these are the most evident manifestation of the solar cycle [12]. The 11-year pseudoperiodic solar cycle, which is now called the Schwabe cycle, is the variation in the number of sunspots over time, and it consists of a pseudoperiodic process with a period of between 9 and 13 years, and strong erratic fluctuations [11,13,14]. The apparently surprising finding that TSI is stronger at sunspot number maxima is explained by the contemporary growth of solar activity which increases the radiation from bright faculae and plages that appear on the solar surface associated with solar active regions. This increase in radiation outweighs the dimming produced by sunspots.

A number of nonlinear models for this process have been proposed, including limit cycles, chaotic maps, and stochastic turbulent processes. The latter two approaches give solutions in agreement with the observation that the asymptotic waiting time distribution of solar flares is well fitted by either an inverse power-law distribution [15–17] or a Lévy distribution [18]. Note that because the Lévy distribution has an asymptotic inverse power-law behavior, as will be explained in Sec. IV, the two distributions yield equivalent stochastic properties.

The frequency variability of solar flares is significant for our study because herein we hypothesize that solar flare frequency is higher in concomitance with an increased TSI. The sun's irradiance varies from day to day mainly in response to the changing projected area and evolution of dark sunspots and very bright faculae [13] that appear and disappear, giving rise to a TSI intermittentlike behavior. An unusually bright flare can temporarily increase the TSI by about 1% [13] but, in general, solar flares last on average only for a few minutes [13]. Therefore, only a small fraction of TSI is associated with solar flares. However, the concomitant presence of the 11-year solar pseudoperiodic cycles in both TSI and solar flare frequency makes it reasonable to suppose that during periods of higher solar activity, when the solar active regions are slightly hotter and/or larger and more numerous, the increased solar activity also induces an increase of the solar flare frequency as a kind of by-product, at least in a stochastic sense. Therefore, even if solar flares cannot directly account for the irradiance increase over the solar cycle, we suppose that the time evolution of their occurrence contains significant stochastic information about solar dynamics. That is, we hypothesize that solar flare intermittency is coupled to and, therefore, *mimics* the solar surface intermittency.

So we suppose that the TSI fluctuations present temporal intermittent patterns that are stochastically in accordance with the solar flare intermittency: the greater the frequency of solar flares, the more intense is the total solar activity and, therefore, the sun's irradiance on the earth. This variation in solar activity induces similar 11- and 22-year pseudoperiodic cycles in the earth's average temperature, as well as trends that move the average temperature up or down for tens or even hundreds of years [10,11,13]. The coupling to short-term (monthly) changes in the global temperature is less evident than those that track the long-term solar cycles, since one would anticipate that these short-time temperature fluctuations should inherit the same intermittent dynamics of solar activity. Traditional measures, such as cross-correlation functions, would not show the connection between short-time fluctuations of the global temperature and solar flare activity, because of strong nonlinear hydrodynamic interactions across the earth's surface. For example, the hydrodynamic interaction of the atmosphere over land and water would suppress any direct correlation between the intermittent irradiance of the sun and the earth's short-time response.

We do not have a system of primitive equations to describe the dynamics of the coupled earth-sun system, so we must extract as much information as possible from data. We use five mean monthly temperature data sets (global, North, South, over land, and over ocean regions) that cover the period from 1856 to 2002. However, we do not analyze these data sets blindly, but are guided by the nonlinear dynamics that would be produced by the observed intermittency in a time of solar flare activity.

The basic idea is that the fluctuations of the TSI, supposed coupled to the solar flare intermittency, induce a scaling behavior in the global temperature fluctuations. Said differently, we expect temporal persistence in the alternate intervals of higher and lower global temperatures with an inverse power-law waiting time distribution, because of the inverse power-law character of the solar flare intermittency. Considering a solar flare as an event, the time series for the number of solar flares has been interpreted as a waiting time interval between events. The solar flare waiting time distribution function is determined to be an inverse power-law probability density function [15–17]. Such dynamical stochastic processes can be described by generalizations of random walks. A *Lévy flight*, for example, is such a process with a diverging

second moment. A *Lévy walk*, on the other hand, visits the same spatial sites as does a Lévy flight, but each step takes a finite time and the second moment is finite. The time necessary to complete a step in a Lévy walk is specified by an inverse power-law waiting time distribution, as first discussed by Shlesinger *et al.* [19,20]. It has been determined [15] that a Lévy walk can describe the intermittent solar flare signal. Scafetta and Grignoli [21] established that, in general, the presence of a Lévy-walk process in a given time series can be determined by the joint use of two separate scaling processing techniques, the diffusion entropy analysis (DEA) and the standard deviation analysis (SDA). We apply the same approach to the analysis of temperature data sets and compare the results with the Lévy-walk statistics induced by solar flare intermittency.

The DEA was developed as an efficient way to detect scaling and memory in time series for variables in complex systems. This procedure has been successfully applied to sociological [22], astrophysical [15], and biological [23] time series. Moreover, the joint use of the DEA and SDA has shown the Lévy-like nature of the long-range persistence of the purine and pyrimidine bases in DNA sequences [24–26]. The joint use of DEA and SDA will establish that the Lévy-walk statistical properties of solar flares are manifest in the earth's global temperature fluctuations.

We note that there are two separate scaling exponents of interest to us in this case. The first has to do with the probability density function $p(x,t)$, where x is the variable of interest and t is the time. The first scaling property has the form

$$p(x,t)=\frac{1}{t^{\delta}}F\left(\frac{x}{t^{\delta}}\right), \tag{1}$$

where δ is the first scaling exponent. The second scaling index is associated with the standard deviation of the process of interest and is given by

$$\sqrt{\langle(x-\overline{x})^2;t\rangle}\propto t^{H}, \tag{2}$$

where H is the Hurst exponent. As is explained in detail in Ref. [21] and briefly summarized in Sec. IV, these two exponents can be obtained using the DEA and SDA methods independently. It has been shown [21] that if a time series is characterized by Gaussian statistics, the two scaling exponents are identical, that is, $\delta=H$. If, instead, the process under study is characterized by Lévy-walk statistics, the two scaling exponents δ and H can be related by

$$\delta=\frac{1}{3-2H}=\frac{1}{\alpha}, \tag{3}$$

where α is the Lévy exponent defined in Eq. (12) in Sec. IV. We refer to Eq. (3) as the Lévy-walk diffusion relation. The assessment of this property, that is, the comparison between the values of the exponents δ and H measured for the earth's temperature and their relation to the scaling exponents measured for the hard x-ray solar flare waiting time series, is used in this paper to prove the conjecture that the earth's global temperature inherits the intermittent, Lévy-like nature of solar flares within the temporal range from a few weeks to a few years.

The long-term cross-correlation analysis between the earth regions (North-South and land-ocean) and the TSI is based upon a multiresolution analysis via the maximal overlap discrete wavelet transform (MODWT) [27]. The MODWT decomposes a data set into smooth, detailed, and residual components associated with particular temporal scales. This analysis establishes that the solar cycles and long-period trends have significant influence on the earth's temperature, with differences among the four earth regions. These differences are traced back to the different responses of these separate regions to the solar activity. This analysis also shows that the traditional method of correlation analysis [10], even as adapted herein to the multiresolution wavelet analysis, may suffer from significant limitations.

The outline of the paper is as follows. In Sec. II, we illustrate the time series under study and highlight their main properties. Section III is devoted to the wavelet multiresolution analysis of the time series and to the study of the correlations between global North-South hemisphere and land-ocean region temperature anomalies on a hierarchy of temporal scale. We also study the correlation between these temperature data sets and the TSI reconstruction during the same periods. Section IV shows the implementation of the DEA and SDA on the data and presents an interpretation of the results in light of the determined stochastic properties of the solar flare activity. A computer-based model is presented to simulate the response of the earth to the solar flare intermittency. Finally, in Sec. V we compare and contrast the results obtained using the various methods.

II. EARTH TEMPERATURE ANOMALIES

The term *temperature anomalies* is a technical definition adopted in the current literature on earth's weather and climate processes to denote the departure of air and sea temperature from the 1961–1990 mean temperature value. The data analyzed are updated continuously by institutions such as the Climate Research Unit [28] and the Hadley Center for Climate Prediction and Research, Meteorological Office [29]. The earliest attempt at collecting these data was done in 1986 [30] and has culminated in what is recognized as one of the most accurate data files for global air temperature and global sea-surface temperature (SST) [31].

The basic data set of global earth temperature anomalies (HADCRUT) is a combination of land-air temperature anomalies [32] (CRUTEM1) and sea-surface temperature anomalies [33] on a 5°×5° grid-box basis. The merging of the two data sets was discussed by Parker *et al.* [33] and more recently by Jones *et al.* [34]. The land surface time series are calculated using data from the Global Historical Climatology Network (Version 2) and sea-surface temperature anomalies from the United Kingdom MOHSST data set and the NCEP optimum interpolated SSTs (Version 2). The data set has been extensively used in the various Intergovernmental Panel on Climate Change (IPCC) reports (see, e.g., Nicholls *et al.* [35]). An absolute temperature climatology is also available (de-

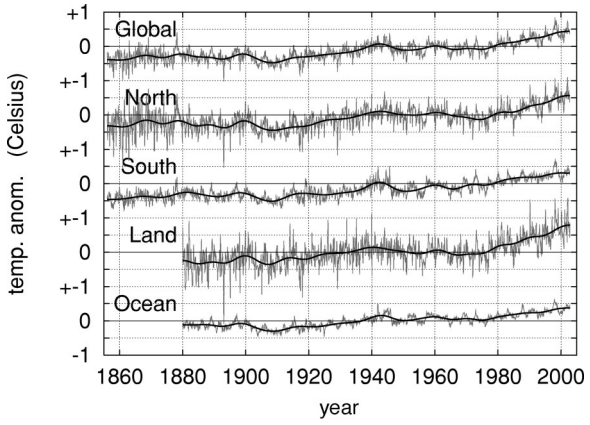

FIG. 1. Global and local earth temperature anomalies in degrees Celsius (years 1856–2002). The smooth lines are the wavelet multiresolution smooth curves S_6.

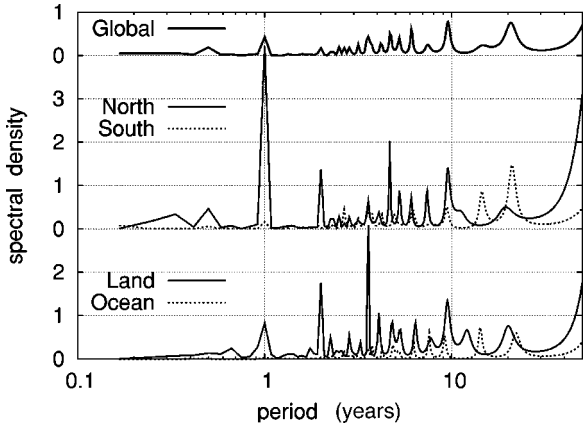

FIG. 2. Global and local earth temperature anomaly spectral density analysis against the period; mean of maximum entropy spectral estimation with 500 poles, arbitrary units.

tails in Jones *et al.* [36]). The land-air temperature has been corrected for nonclimatic errors, such as changes in the location of the weather stations and changes in instrumentation [32]. The SST data have been corrected for changes in instrumentation that was used before 1942 [33,37–39]. The data that we actually analyze are mean monthly temperature anomalies that can be downloaded from the Climatic Research Unit, U.K. [40] (Global and North-South temperatures, period 1856–2002) and from the National Climatic Data Center U.S.A. [41] (land-ocean temperatures, period 1880–2002).

Figure 1 shows the five temperature anomaly data sets, from which the similarity in the curves is evident. The smooth lines are the wavelet multiresolution S_6 smooth curve of the signal (see Sec. III for a detailed explanation about the multiresolution analysis). The S_6 smooth curve is a convenient way to establish a certain kind of mean value to center the temperature fluctuations. In fact, the S_6 smooth curve is obtained by a wavelet average of the data over a time scale of $2\tau=2^6=64$ months. From 1860 to 1915 the average global earth temperature is almost constant, with a change of only 0.2 °C. From 1915 to 1945 the temperature increased by 0.6 °C. From 1945 to 1980 the average temperature remained approximately constant again. Finally, from 1980 to the present time there is a further increase in the average temperature of almost 0.4 °C. It is interesting to observe that the Northern hemisphere and the land temperature data sets appear more noisy than the Southern hemisphere and ocean temperature data sets, respectively. This phenomenon is probably due to the fact that the Northern hemisphere contains most of the earth's land, while the Southern hemisphere contains most of the earth's oceans. In fact, the high heat capacity of water reduces the temperature fluctuations of the oceans. We expect that the climate over land will be more random than that over the ocean, because in contrast to the relative homogeneity of the ocean's surface, the land presents deserts, forests, valleys, and mountains, making its temperature less correlated than that of the nearly homogeneous ocean. The data also show that during the period 1980–2002, the temperature over the land increased by an average of almost 0.6 °C, while the temperature over the ocean increased by only 0.3 °C. This effect is probably related to the higher effective heat capacity of water compared with that of land, but a small contribution to this land warming from human technology cannot be excluded.

Figure 2 shows the spectral densities of the five temperature anomalies as a function of time period, expressed in years. The power spectrum is estimated by the maximum entropy method (MEM) [42,43] with 500 poles. We adopt the MEM because it is more accurate than the (fast) Fourier transform method or than the Lomb normalized periodogram [42,43] in estimating the power spectrum of evening sampled data. In fact the adoption of poles can provide an accurate representation for underlying power spectra that have sharp, discrete lines; see Refs. [42,43] for details. Because the power spectra of all temperature data sets were estimated with the same method and the values on the *y* axis are plotted with the same units, we suggest that the significance of the peaks can be evaluated by comparing their relative amplitudes. The dominant periodicities involve time periods 12 months long (related to the yearly cycle of the earth orbiting the sun), ~10 years long, and 21–22 years long, and several harmonics or pseudoperiodicities. The main cycles are all established solar cycles, with the Schwabe pseudoperiodic cycle being the most widely known; the (21–22)-year cycle, known as the Hale cycle, is believed to be due to a magnetohydrodynamic dynamo action that periodically regenerates the solar magnetic field [11,13,14,44].

Again, we notice a similarity between the Northern hemisphere and land regions and the Southern hemisphere and ocean regions. It is also interesting to observe that the annual periodicity is very prominent for the Northern hemisphere, which contains most of the land, and is very weak for the ocean region. Here again the explanation may be the high effective heat capacity of the water associated with the global ocean circulation that moves water between the Northern and Southern hemispheres. For example, two well known phenomena associated with the interaction between the atmosphere and ocean circulation are the El Niño Southern Oscillation and the North Atlantic Oscillation [4]. The power spectra for all temperature data sets show several peaks with periods between two and seven years and also a peak at 14

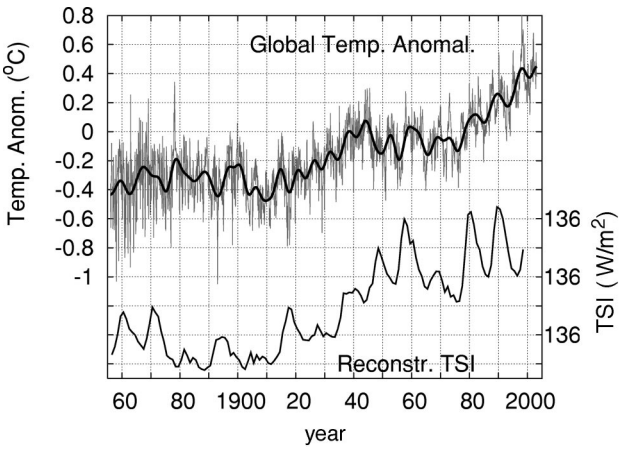

FIG. 3. Global temperature anomalies against annual reconstruction of TSI based on the sunspot number. The figure clearly shows the Schwabe or 11-year solar pseudocycles. TSI slightly increases during the period 1910–2000.

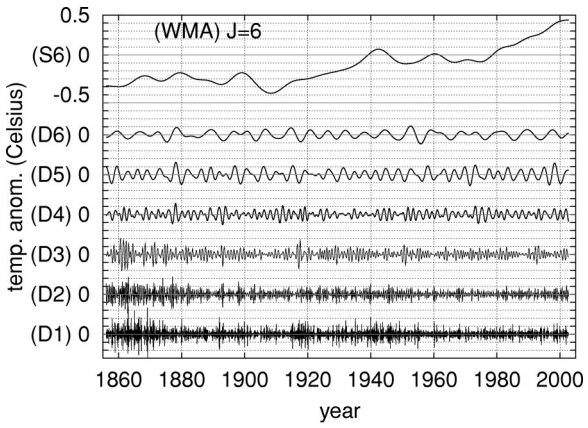

FIG. 4. WMA, with $J_0=6$, of the global earth temperature anomalies during the period 1856–2002.

years for the Southern hemisphere and ocean. All these peaks can probably be associated with circulation phenomena too, because they seem to affect the earth regions differently, but a contribution due to some minor solar cycles cannot be excluded [14]. Note that the periods of about 10 and 21–22 years are supposed to depend on the Schawbe and Hale solar cycles. Their statistical significance is made clear by the power spectrum concerning the global temperature, where the amplitudes of the corresponding peaks are higher than those of all the other peaks. Such behavior is less manifest in the spectra of all local temperature sequences. A valid reason may be that the amplitudes of the annual cycle and of the several pseudocycles associated with the thermodynamic interactions between the atmosphere and ocean are, in part, compatible with or sometimes higher than those induced by the two main solar cycles.

To emphasize the relation between the earth's temperature and solar activity, in Fig. 3 we display the global temperature anomalies against the mean annual reconstruction of the TSI, based on the number of sunspots during the period 1860–2000 [9]. A recent study of the spectrum of the sunspot number sequence using the continuous wavelet transform can be found in Ref. [14]. The TSI reconstruction shown in Fig. 3 describes the radiant energy emitted by the sun over all wavelengths that falls per second on $1\,\mathrm{m}^2$ outside the earth's atmosphere normalized to the mean earth-sun distance (1 AU) [45]. The figure, where the presence of the Schawbe cycle is evident, shows also a definite tendency for the solar activity to increase, especially during the time period 1910 to 1950, although to a smaller extent this increase is also observed in the period from 1980 to 2000 (see Ref. [58]). It is plausible, as the figure shows, that this increasing solar activity has contributed to the increase in the earth's global temperature taking place in the same time periods.

III. WAVELET MULTIRESOLUTION ANALYSIS

The broad spectrum of variation in the global temperature time series suggests that we analyze these data using wavelet transforms. Wavelet transform [27,46] analysis makes use of functions, the wavelets, which are localized in both time and frequency. There exist continuous and discrete versions of the wavelet transform. We make use of wavelet multiresolution analysis (WMA) via the MODWT [27]. It is possible to prove [27] that, given an integer J_0 such that $2^{J_0}<N$, where N is the number of data points, the original time series represented by the vector $\mathbf{X}$ can be decomposed as follows:

$$\mathbf{X}=S_{J_0}+\sum_{j=1}^{J_0} D_j\,, \tag{4}$$

$$S_{j-1}=S_j+D_j\,. \tag{5}$$

The D_j detail represents changes on a scale of $\tau=2^j$, that is, it captures all fluctuations with a period between 2^j and 2^{j+1} time units, while the S_{J_0} smooth curve represents averages on a scale of $\tau=2^{J_0}$. The scaling coefficient τ characterizes the width of a wavelet. We define the wavelet *residuals* as

$$R_{J_0}=\mathbf{X}-S_{J_0}=\sum_{j=1}^{J_0} D_j\,. \tag{6}$$

It is then evident that we can interpret the residuals as fluctuations about the local mean value evaluated on the time scale $\tau=2^{J_0}$.

Figure 4 shows the WMA, with $J_0=6$, of the global earth temperature anomalies during the period 1856–2002. Note that the integers here correspond to months. The analysis is done by using the 8-tap Daubechies *least asymmetric* scaling and wavelet filter [27]. According to Eq. (4) the sum of all curves of Fig. 4 gives the original data set. The S_6 smooth curve gives an excellent mean trend of the data. We observe that the D_6 detail contains most of the (9–13)-year cycle and the D_3 detail contains most of the one-year cycle.

Figure 5 shows the WMA, with $J_0=6$, of the other four temperature data sets. We observe that the D_1, D_2, and D_3 fluctuations for the four data sets are significantly different from one another. More specifically, the temperature fluctuations in the Northern hemisphere and over the land appear to be larger than those over the ocean and in the Southern hemi-

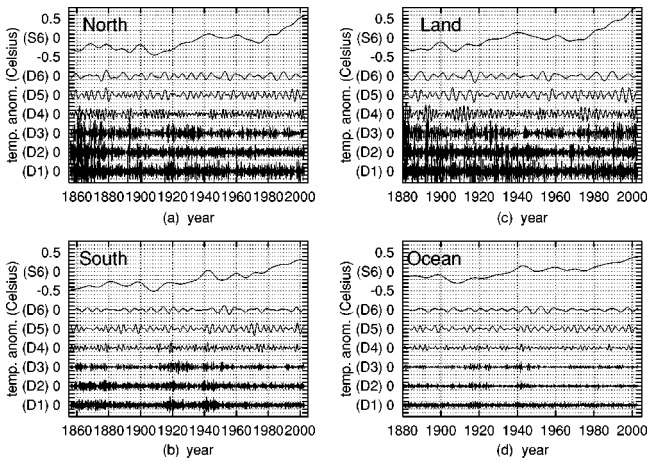

FIG. 5. WMA, with $J_0=6$, of the four regional earth temperature anomalies.

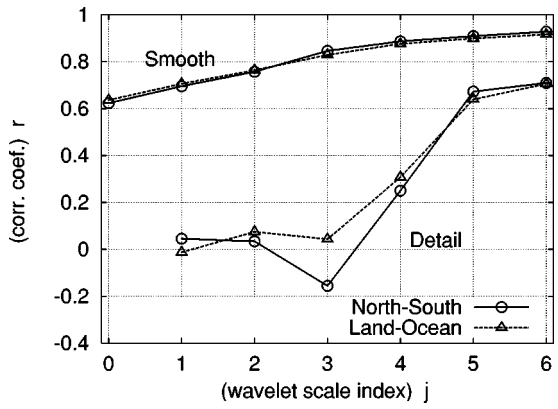

FIG. 6. Correlation coefficient r of smooth and detail components between Northern and Southern hemispheres and between land and ocean regions.

sphere. On the other hand, the D_5 and D_6 detail curves have almost the same amplitudes for the four data sets and look somewhat similar. This analysis suggests that the fluctuations with a temporal scale $\tau > 2^5 = 32$ months express global temperature properties, while the fluctuations at a temporal scale $\tau < 2^5 = 32$ months are more influenced by local temperature properties.

Multiresolution correlation analysis

Multiresolution correlation analysis via wavelets [47] evaluates the correlation between pairs of partners (smooth, residual, or detail curves) obtained via the WMA. For any given pair of data sets (x_i, y_i), $i=1,\ldots,N$, the linear correlation coefficient r is given by the formula

$$r = \frac{\sum_i (x_i-\overline{x})(y_i-\overline{y})}{\sqrt{\sum_i (x_i-\overline{x})^2}\sqrt{\sum_i (y_i-\overline{y})^2}}, \tag{7}$$

where, as usual, $\overline{x}$ is the mean of the former sequence and $\overline{y}$ is the mean of the latter sequence. The value of r lies between -1 (negative correlation) and 1 (positive correlation). A value of $r \approx 0$ indicates that the variables x and y are uncorrelated.

Figure 6 illustrates the correlation coefficient r of smooth and detail components between Northern and Southern hemispheres and between land and ocean regions shown in Fig. 5. The figure shows that the small details D_1, D_2, and D_3, which approximately cover a temporal scale up to one year, are not significantly correlated. The D_3 details between North and South are even slightly anticorrelated. This anticorrelation is a consequence of the D_3 detail containing most of the annual cycle, but the Northern and Southern hemispheres having inverted seasons. The D_5 and D_6 details show a significant correlation with a probability above 99%. Therefore, because these details are included in the S_4 and S_5 smooth curves, respectively, we suggest that the S_4 and S_5 smooth curves are the best curves to indicate the global correlation among the various earth regions. However, we notice that the smooth curves do not yield a substantial change of correlation upon increase of the index j. We think that the large correlation values that the smooth curves reach at $j > 6$ do not carry any significantly new information with respect to the smaller values of the index j. For this reason we focus our attention on the details, which in fact show a much larger change in correlation intensity when moving from small to large values of j.

Figure 7 shows a detailed comparison between the S_5 smooth curve of the Northern hemisphere and the corresponding curve of the Southern hemisphere, and between the S_5 smooth curve of the land and the corresponding curve of the ocean. The S_5 smooth curves are obtained by using $S_5 = S_6 + D_6$, [see Eq. (5)], and contain the 11-year pseudoperiodic cycles induced by the sun. These curves illustrate a behavior similar to the reconstructed TSI shown in Fig. 3. In all five cases and in the specific case of the ocean, we find remarkable correspondence between the maxima of the S_5 smooth curve and those of the TSI that characterizes the 11-year solar cycle. In particular, note the good correspondence of the maxima of the four last cycles which occurred approximately in 1959, 1970, 1981, and 1991. This figure also shows a good correspondence with the irradiance curves

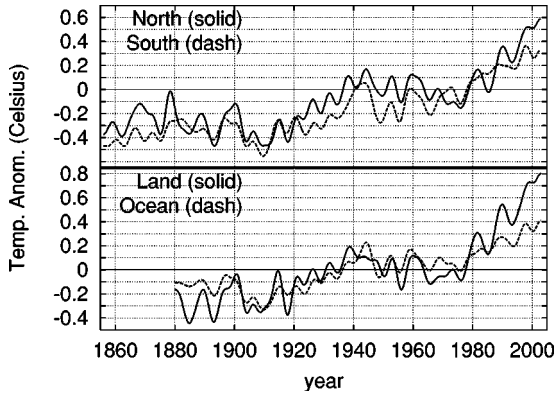

FIG. 7. Comparison of S_5 smooth curves regarding the North-South hemispheres and land-ocean regions.

TABLE I. Correlation coefficient r between the TSI and the wavelet smooth curves of the temperature data sets.

	Global	North	South	Land	Ocean
S_4	0.76	0.72	0.75	0.69	0.78
S_5	0.80	0.77	0.78	0.74	0.82
S_6	0.82	0.77	0.80	0.77	0.84

of Fig. 3. In both cases we find that in the period of time from 1910 to 1950 and in that from 1980 to 2000 the solar cycle yields oscillations about a mean temperature value significantly increasing with increasing time. In Table I we report the coefficient of correlation between the TSI and the S_4–S_6 smooth curves of temperature, in several cases. The smooth curves for the ocean temperature are more correlated with the TSI, while the land region is less correlated. However, the correlation between TSI and the S_4–S_6 smooth curves of all earth regions is always significant: we obtain $r \approx 0.8$ and the probability that the two data sets are correlated is above 99%.

Also we observe that the Northern hemisphere is slightly warmer than the Southern hemisphere. This may be due to the higher effective heat capacity of water, but it may also be due to the small effects of the ellipticity of the earth's orbit and the inclination of the earth's axis of rotation. Moreover, because of the hydrodynamic interaction of the atmosphere over land and water, if in a given time region the temperature over land is greater than that over the ocean, immediately afterward the opposite effect takes place, and the temperature over the ocean is greater than that over the land. In fact, the land-ocean S_5 smooth curve of Fig. 6 shows that in the time regions of persistent temperature increase (1910–1950 and 1980–2000) the temperature over the land is greater. Instead, in the time regions of persistent temperature decrease (1880–1910 and 1950–1980) the temperature over land is less than that over the ocean.

IV. SCALING ANALYSIS

In the previous section we studied the correlation among the temperature fluctuations of different regions of the earth and the TSI. In particular, using a standard technique, we obtained a significant correlation between temperature details with a time scale larger than a few years, but we did not find any significant correlation ($|r| < 0.15$) within time scales up to a few months. This lack of short-time correlation among different regions of the earth may suggest that the fluctuations in solar activity do not have a significant influence on the earth's short-time temperature fluctuations. However, this need not be the case. The data illustrated in Figs. 1 and 5 suggest that each region of the earth is subject to a different type of random fluctuation. Moreover, Fig. 7 suggests that similar temperature properties may appear in different regions with a random time shift, this being a reasonable consequence of the hydrodynamic interaction of the atmosphere over land and water, but also that different earth regions respond in different ways to the same solar action. The correlation method could mistake these effects for a lack of correlation at short time scales, as Fig. 6 shows. Therefore, the traditional correlation method of analysis may not properly reflect the true nature of the phenomenon under study.

To overcome this limitation, in this section we address the issue of establishing whether the temperature fluctuations are characterized by some type of memory, under the specific form of scaling properties that survive for at least from one month to a few years. We investigate whether these scaling properties take the form of fractional Gaussian statistics or of Lévy statistics. The latter statistics, as we mentioned, were found to properly describe solar flare activity [15]. Therefore, if the temperature fluctuations were shown, in a convincing way, to mirror the Lévy statistics induced by the solar flares, that would be strong evidence for the direct coupling of global temperature and solar activity. In fact, as we pointed out in the Introduction, the solar flare frequency is expected to be a sufficiently good indicator of solar activiy.

Before illustrating the results supporting our conjecture, we present a short review of the basic issues concerning this problem. We build up an artificial sequence that simulates the occurrence in time of artificial solar flares [15] and evaluate the solar flare frequency sequence, that is, the sequence of the number of solar flares that occur for a given time interval. This sequence provides a model for an artificial monthly mean TSI sequence that is supposed to drive the monthly mean air temperature anomalies. We use this model to prove that the joint use of DEA and SDA can detect that the Lévy scaling coefficient embedded in the solar flare sequence is transmitted to the earth's temperature sequences.

A. How to reveal Lévy scaling

Scale invariance has been found to hold empirically for a number of complex systems [48], and the correct evaluation of the scaling exponents is of fundamental importance in assessing if universality classes exist [50]. The DEA and SDA techniques are based on the prescription that the numbers in a time series $\{\xi_j\}$ are the fluctuations of a diffusion trajectory (see [15,21–25,49,51] for details). Therefore, according to the prescription of Ref. [21], we shift our attention from the time series $\{\xi_j\}$ to the probability distribution function (PDF) $p(x,t)$ or the corresponding diffusion process. Here x denotes the variable collecting the fluctuations and is referred to as the diffusion variable. The scaling property takes on the form

$$p(x,t) = \frac{1}{t^{\delta}} F\left(\frac{x}{t^{\delta}}\right), \tag{8}$$

where δ is the scaling exponent. The DEA [21] is based on the evaluation of the Shannon entropy $S(t)$ using the PDF (8). If the scaling condition of Eq. (8) holds true, it is easy to prove that

$$S(t) = -\int p(x,t)\ln[p(x,t)]dx = A + \delta \ln(t), \tag{9}$$

where A is a constant.

There are two main forms of anomalous diffusion. The first is the generalization of Brownian motion proposed by Mandelbrot [48], known as fractional Brownian motion (FBM) and yielding for the diffusion process a standard deviation (see the SDA [21]) that scales in time as

$$D(t)=\sqrt{\langle x^2;t\rangle-\langle x;t\rangle^2}\propto t^H. \tag{10}$$

This kind of anomalous diffusion fits the scaling definition of Eq. (8) with $\delta=H$ because $F(y)$ is a Gaussian function of y [21].

A second form of anomalous diffusion is obtained by generalizing the central limit theorem (CLT) [52,53]. The prescriptions of the generalized central limit theorem (GCLT) are as follows. Let us assume that the diffusing variable x is the sum of t independent random variables η_i, positive or negative, each of which has a probability distribution, symmetric around $\eta=0$. Let us assume also that for large values of $|\eta|$, this distribution is an inverse power law, with index $\mu>1$. We assign to it the following analytical form:

$$\psi_\eta(\eta)=\frac{1}{2}(\mu-1)\frac{T^{\mu-1}}{(T+|\eta|)^\mu}, \tag{11}$$

where T is a positive constant introduced to avoid short-time divergences and to set the normalization condition. Note that $2<\mu<3$ ensures that, although the first moment of $\tau=|\eta|$ is finite, the second moment of τ is not. This divergence of the second moment violates the conditions necessary for the CLT. Then, according to the GCLT, for $t\to\infty$, the diffusion becomes stable and the Fourier transform of $p(x,t)$ approaches the Lévy form

$$\hat{p}(k,t)=\exp(-b|k|^\alpha t), \tag{12}$$

where $b=T^{1/(\mu-1)}$ is a generalized diffusion coefficient, determined by the strength of the fluctuations, and $\alpha=\mu-1$. The stable form of Eq. (12) yields scaling, namely, it fits the condition of Eq. (8), and the scaling coefficient δ is given by

$$\delta=\frac{1}{\alpha}=\frac{1}{\mu-1}. \tag{13}$$

In the recent literature [19,20] frequent use is made of the Lévy-walk model. The main idea of a Lévy walk is that the random walker takes a step in a time proportional to $\tau=|\eta|$, forward or backward, with the same intensity. We adopt the Lévy-walk model and replace the distribution Eq. (11) with the corresponding time distribution

$$\psi(\tau)=(\mu-1)\frac{T^{\mu-1}}{(T+\tau)^\mu}. \tag{14}$$

The special form of Lévy walk we adopt here is that originally proposed in Ref. [49], which later [15] turned out to be especially convenient to analyze the solar flare waiting time distribution. The solar flare activity consists of impulses separated by a waiting time interval whose distribution can be well fitted by Eq. (14). Thus, it is convenient to force the random walker to always step in the same direction and by the same amount any time an event occurs. Therefore, we find it convenient to adopt the same random walk prescription that provided an efficient method of analysis of solar flares [15], since the main purpose of this section is to establish that air temperature anomalies inherit the Lévy statistics of solar flares.

Thus, we proceed as follows. Given a sequence $\{\tau_j\}$, with $j=0,1,\ldots,$ of random time intervals distributed according to Eq. (14), we build up a new time series $\{\xi_i\}$ with the following prescription. The discrete time i runs from 0 to the maximum possible value allowed by the data under study, and ideally to infinity. At the integer time i at which an event occurs, we set $\xi_i=1$. For integer times at which no event occurs, we set $\xi_i=0$. It is evident than the times with no events are much more numerous that the times with an event. The times with events are given by $i=[\Sigma_{j=1}^m\tau_j]$, where $[a]$ denotes the integer part of a. The times at which no event occurs fit the condition $[\Sigma_{j=1}^m\tau_j]<i<[\Sigma_{j=1}^{m+1}\tau_j]$. This time series generates a diffusion process with a scaling given by $\delta=1/(\mu-1)$ for $2<\mu<3$, namely, by Eq. (13).

This particular approach to Lévy statistics yields a diffusion process with finite second moments. In fact, by using this procedure the walks, some of which may have very large intensities, are turned into the signal time persistence, lasting for extended times in the case of exceptionally intense walks. Consequently, as shown in Refs. [54,55], the asymptotic time evolution of the second moment has the form of Eq. (10). The power index H can be related to the index μ in such a way as to be associated with δ by means of the Lévy-walk diffusion relation (3), which we rewrite here as

$$\delta=\frac{1}{3-2H}=\frac{1}{\mu-1}=\frac{1}{\alpha}. \tag{15}$$

In the Introduction we pointed out that the joint use of the DEA and SDA independently determines δ and H, and therefore provides a compelling method for establishing the Lévy nature of the statistical process under study by checking the validity of Eq. (15). Here we limit ourselves to pointing out that the assessment of this property is used to verify the conjecture that air temperature anomalies inherit the Lévy nature of solar flares.

B. Artificial sequences as an illustrative example

With the help of the earlier theoretical remarks we can address the important issue of a stochastic model for air temperature anomalies [56]. This is done as follows. We first create a sequence $\{\xi_i\}$, which can be considered as a model for solar flares. Then we derive from this sequence a further sequence $\{f_t\}$, whose values are obtained by recording the frequency of events of the earlier sequence. We make the assumption that the air temperature fluctuations are proportional to the values of this new sequence because the higher the solar flare frequency the higher the solar activity. We restate an important aspect discussed in the Introduction. The solar flare intermittency is not the direct cause of the earth temperature fluctuations, since the radiation energy of the

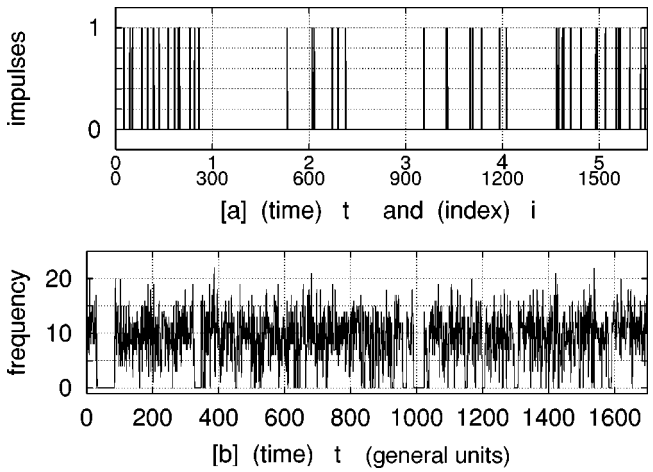

FIG. 8. Computer-generated intermittent sequence of impulses with a Lévy waiting time distribution with $\alpha=1.5$. The sequence ξ_i is always zero except at the occurrence of the event, when $\xi_i=1$. The time t indicates the temporal units, while the index i indicates the position in the time series. (a) shows the first $300\times5.5=1650$ data points which correspond to the first 5.5 time units. (b) shows the frequency of impulses for each unit of time. This last sequence counts 1700 data points for 1700 time units obtained from a $1700\times300=510\,000$ long data set $\{\xi_i\}$ of the type of (8a).

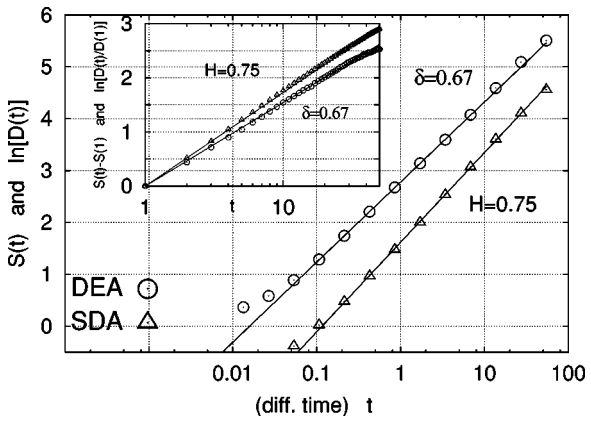

FIG. 9. DEA and SDA of the Lévy-walk sequence shown in Fig. 8. The large picture refers to the analysis of the original 510 000 data point sequence $\{\xi_i\}$. The small picture refers to the analysis of the 1700 data point frequency sequence shown in Fig. 8(b). The two straight lines show the two theoretical scaling coefficients $\delta=0.67$ and $H=0.75$ for $\alpha=1.5$. [Note that for the SDA we plot the natural logarithm of $D(t)$.]

solar flares is relatively small. Instead, we suppose that the periods of higher solar activity, when the solar active regions are slightly hotter and/or larger and more numerous, are also characterized by an increased solar flare frequency, at least in a stochastic sense, because solar flares can be seen as a kind of by-product of solar activity. In other words, we hypothesize that all solar phenomena are coupled in such a way that it is sufficient to study the dynamical evolution of one of the solar phenomena, in this case the solar flare waiting time series, to have a reliable stochastic representation of the evolution of the entire solar activity and, therefore, of the TSI that ultimately heats the earth and drives its temperature. Thus, we suppose that the artificial solar flare frequency series $\{f_t\}$ is virtually the model for the air temperature anomalies.

Let us see how this is done in practice. First, we generate a sequence τ_j of positive numbers distributed according to a Lévy distribution with $\alpha=1.5$ and $b=20$ that produces diffusion effects equivalent to those of the inverse power distribution Eq. (14) with $\mu=\alpha+1=2.5$ and $T=b^\alpha=90$. Then we build a sequence of 510 000 data points $\{\xi_i\}$ according to the earlier rule, that is, $\xi_i=0$ almost always except at the occurrence of the event when $\xi_i=1$. This is our model to simulate the occurrence of solar flares. The numbers $i=1,2,\ldots,$ are measured in natural units of τ_j. Figure 8(a) shows the first 1650 data points of this long sequence. Then we choose a time unit, for example, such that 1 time unit=300 natural units. In the temperature data the time unit is one month. Therefore, Fig. 8(a) shows the first 5.5 time units of the sequence. In Fig. 8(b) we show the frequency of impulses for each time unit. The frequency time series $\{f_t\}$ contains 1700 data points. In conclusion, Fig. 8(a) illustrates the model for solar flares and Fig. 8(b) the model for mean monthly temperature anomalies, which should evidently be closely related to the frequency sequence of solar flares. However, the number of data points on temperature anomalies is much less than the number of data points for solar flares. Instead, the number of data points for the artificial temperature anomalies produced in this example is comparable to that for real data, discussed in the next subsection.

We now apply the DEA and SDA to both the artificial solar flares and artificial temperature anomaly time series of Fig. 9. The results of this analysis are fitted with straight lines of the type of Eqs. (9) and (10), yielding the two theoretical scaling coefficients $\delta=0.67$ and $H=0.75$ for $\alpha=1.5$ obtained by using Eq. (3). The large graph refers to the analysis of the original 510 000 data point sequence $\{\xi_i\}$. The inset depicts the analysis of the 1700 data point frequency sequence $\{f_t\}$, shown in Fig. 8(b). The two graphs in Fig. 9 show a very good agreement with theory. In particular, we stress that the SDA and DEA plots, shown in the small inset, are obtained with the shorter data set having a length compatible with the mean monthly temperature data sets. Therefore, in the diffusion time interval $1<t<50$, the statistics generated by $N=1700$ data points is rich enough to obtain a satisfactory PDF and, consequently, reliable scaling properties. The small inset of Fig. 9 shows the typical bifurcation associated with the two scaling laws that characterize Lévy-walk statistics.

The results of Fig. 9 confirm an important property of scaling, that being that the long sequence of 510 000 values corresponding to the solar flare activity and the short sequence of 1700 values expressing the intensity of temperature fluctuations yield the same anomalous statistics, of Lévy type, with the same accuracy. This result is a consequence of the fact that in the latter case the temperature intensity is proportional to the number of solar events occurring in the given unit of time, and consequently the random walker moves in the time unit by a space quantity proportional to that of the random walker of the former sequence. The two

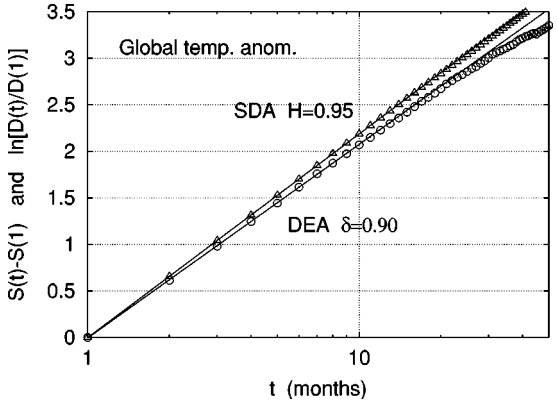

FIG. 10. DEA and SDA of the global temperature anomalies. The error for the two scaling exponents is ± 0.02.

diffusion trajectories are equivalent, and consequently the diffusion algorithm [21] yields the same statistics with the same accuracy. Therefore, Lévy diffusion can be realized on the basis of only 1700 data points, a fact that at first sight might seem questionable. In the same way, the fact that the monthly mean temperature fluctuation is associated to the occurrence of a large number of solar flares makes this apparently meager sequence equivalent to the sequence of solar flares, and consequently statistically rich enough to detect Lévy statistics.

C. Scaling analysis of temperature anomalies and their affinity with the solar flare intermittency

Now we are ready to apply the DEA and SDA to the temperature data sets and, with the help of the Lévy-walk model, we can relate the results that we obtain to the turbulent properties of the solar flares, discovered in earlier [15–18]. Figures 10 and 11 show the numerical results obtained by using the DEA and the SDA for all five temperature anomaly data sets. On the ordinate axis we plot $\ln[D(t)/D(1)]$ and $S(t)-S(1)$; thus, all curves start from 0. The straight lines are functions of the type $f(t)=\delta \ln(t)$ for the DEA and $g(t)=H \ln(t)$ for the SDA and become straight lines as a consequence of the linear-log representation we are adopting. For values of t larger than 50, saturation effects due to the limitations in the number of data points appear. The scaling appears after the first month and persists for several months. The values of the scaling exponents H and δ are obtained by fitting the first ten points. We measure for the global temperature, $H=0.95\pm0.02$ and $\delta=0.90\pm0.02$; for the North, $H=0.89\pm0.02$ and $\delta=0.85\pm0.02$; for the South, $H=0.96\pm0.02$ and $\delta=0.91\pm0.02$; for the land, $H=0.88\pm0.02$ and $\delta=0.84\pm0.02$; for the ocean, $H=0.98\pm0.02$ and $\delta=0.93\pm0.02$.

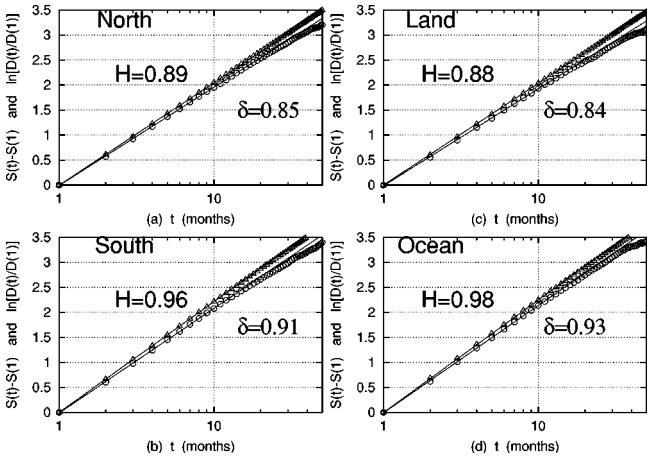

FIG. 11. DEA and SDA of the North-South hemisphere and land-ocean region temperature anomalies. The error for the two scaling exponents is ± 0.02.

The high values of the exponents imply a strong persistence of the temperature fluctuations. This means that the temperature changes gradually month by month. We observe that both scaling exponents δ and H are slightly larger for the Southern hemisphere than for the Northern hemisphere and for the ocean than for the land, indicating a stronger persistence. These effects may again be explained as being due to the higher heat capacity of water than that of land, leading to an increase in temperature persistence. Finally, we note that the standard deviation scaling exponents H are larger than the diffusion entropy scaling exponents δ for all five temperature data sets. This means that the tails of the PDF of the two diffusion processes are slower than those of corresponding Gaussian distributions. The scaling exponents δ and H satisfy the Lévy-walk diffusion relation (3) within the accuracy of our statistical analysis.

These results suggest that Lévy-walk properties emerge from the global and local temperature anomalies, which in turn are related to the intermittency of the solar activity. In fact, the waiting time distribution of solar flares can be fitted with an inverse power-law distribution of the type of Eq. (11) with $\mu=2.14\pm0.05$ [15]. The value of $\mu=2.14\pm0.05$ would imply Lévy-walk statistics with $\delta=0.88\pm0.02$ and $H=0.93\pm0.02$ [Eq. (3)] for an uncorrelated or shuffled data set [15] that would lose any temporal correlation among the solar flares and conserve only their Lévy component. We observe that the above values give a difference $H-\delta=0.05\pm0.02$ that is compatible with the difference between H and δ that we measure for all the temperature data sets. In particular, we have $H-\delta=0.05\pm0.02$ for the global temperature and for both South and ocean regions and we have $H-\delta=0.04\pm0.02$ for North and land regions.

To understand the actual values of H and δ that we measure for the five temperature data sets, first we have to notice that the waiting time sequence of solar flare is also slightly correlated [15]. For the solar flare data, using the DEA we measure $\delta=0.94\pm0.02$, as Fig. 12 shows. We observe that this value of δ is compatible with $\delta=0.93\pm0.02$ measured for the ocean temperature. The ocean, in fact, is the region of the earth that should better follow the solar activity, at short as well as long temporal resolution, for the reasons of extension, homogeneity, and heat capacity discussed earlier. These important properties reduce the occurrence of uncorrelated events in the ocean temperature that would decrease the values of the scaling exponents, as we have already explained above. Also, we observe that the occurrence of uncorrelated

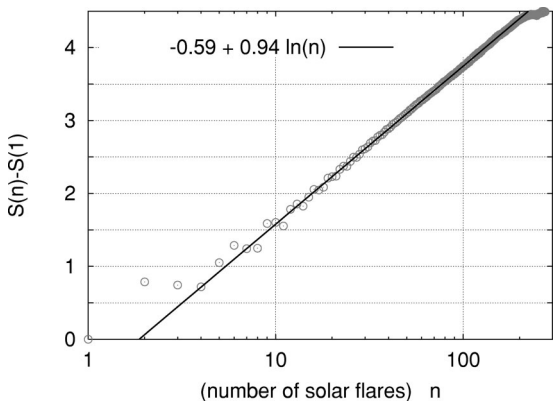

FIG. 12. DEA of the unshuffled waiting time sequence of solar flares during the period 1991–2000. The value of the scaling exponent is $\delta=0.94\pm0.02$.

events would slightly reduce the Lévy-like memory and increase the Gaussianity of the data. This might explain why the difference between H and δ slightly decreases (0.04 against 0.05) for the North and land regions. Finally, we observe that the scaling properties for the waiting time of solar flares persist for 200 consecutive flares, and the waiting time for clusters of 200 solar flares may last for several months. The largest waiting time between two consecutive solar flares during the period 1991–2000 lasted for almost three months, and on average there are nearly 60 solar flares per month [15]. Therefore, the temporal resolution of these clusters is compatible with the temporal range of the scaling of the temperature data sets that persist for at least 20 months, as Figs. 9 and 10 show.

All the above evidence suggests that a Lévy-like intermittency of solar activity induces an anomalous persistence of the alternating periods of high and low temperature on earth. In fact, periods with higher frequency of solar flares correspond to periods with higher solar activity during which the sun is slightly hotter. So the fluctuations of the solar flare frequency should stochastically mimic equivalent fluctuations in the earth temperature, in particular the ocean temperature, according to the simulation made using the simple theoretical model illustrated in the earlier subsection.

V. CONCLUSION

In this paper we study the influence of the solar activity on the earth's temperature. In particular, we focus on how to detect the Lévy nature of the solar intermittency in the temperature monthly mean fluctuations of the Northern and Southern hemispheres as well as in the land and ocean regions.

First, by using the MODWT to decompose the temperature data sets into smooth and detail curves at different temporal scales, we study the *scale by scale* cross correlations between the temperature data sets. This analysis is able to detect global cross correlations only for time scales larger than a few years, but with no significant correlation $(-0.15<r<0.15)$ at time scales of a few months or less. As explained in Sec. IV, this lack of cross correlation between short-time-scale details of the temperature data sets could be mistakenly interpreted as indicating that the fluctuations in solar activity have no observable influence on the short-time fluctuations in the earth's temperature. To overcome this limitation, in Sec. IV we have addressed the issue of establishing whether the temperature fluctuations are characterized by some type of memory that could be associated with the solar intermittency, under a specific form of scaling properties that could survive for at least a few years.

In any case, the MODWT gives an alternative analysis of the temperature data that allows a deep study of the correlation among the main four regions of the earth and confirms known influences of solar activity on the earth's temperature. For example, we recover the 11-year sunspot cycles on the earth's temperature, as well as equivalent long periods of earth cooling or warming that lasted for several decades. We notice that the trend of the TSI during the period 1860–2000 is strongly correlated with the S_5 and S_6 smooth temperature curves.

In particular, the analysis suggests that the increase of the earth's temperature during the last 80 years is partially related to the increase in solar activity. While anthropogenic added greenhouse gases may also have partially contributed to the increase of the earth temperature during the last century [9], we observe that natural phenomena like eruption of volcanoes and several side effects of the solar variability can contribute to climate change [59]. For example, the increased solar activity may favor an increase of the water vapor concentration in the air, which is known as one of the strongest greenhouse gases, as well as the melting of snow and ice, which will lower the reflection of the earth and increase the absorption of solar energy [4]. The increase of the concentration of atmospheric CO_2 and other greenhouse gases may also be partially due to the fact that the warming of the oceans may reduce the uptake of these gases from the air [4]. However, it is still not easy to quantify the contribution to the climate change effect made by natural phenomena against that caused by human industrial activity [57]. The analysis given here shows that during the last 20–30 years the temperature of the land has increased more than the temperature of the ocean, even though the higher effective heat capacity of the water may play an important role in explaining this effect. In any case, the influence of the solar activity on the earth's temperature is also consistent with the presence in the temperature data of long solar pseudocycles such as, for example, the strong 11-year sunspot and solar flare cycle shown by D_6 detail and S_5 smooth curves.

To establish whether the temperature fluctuations are characterized by memory properties that mirror the solar intermittency within a temporal range of a few months, we jointly use DEA and SDA [21]. In fact, the solar flare activity [15] is assumed to reflect the turbulent nature of the dynamics of the sun, through the Lévy-walk model. In fact, since solar flares arise from solar activity, when they are collected, the solar flare frequency time series resembles other solar activity time series like the sunspot number time series, and thus it should provide a good proxy for TSI at least from a stochastic point of view. Also, we observe that such a link between solar flare frequency and solar activity has already been used to estimate the long-time-scale fluctuation of the

TSI before 1600 [13]. In fact, by considering that flares usually occur near sunspot groups and that the aurora borealis below the arctic circle are caused by solar flares, it was possible to estimate the number of sunspots and the TSI by calculating the frequency with which the aurora borealis was seen in Europe [13].

A more direct relation between solar flare frequency time series and TSI for the short-time-scale fluctuation is left to a further study. Herein this hypothesis is indirectly supported by the fact that we have revealed the presence of the Lévy statistics of solar flares in the alternating periods of high and low temperature on earth, in the form of a Lévy walk. In fact, we have shown that the scaling indices δ and H, given by the DEA and SDA, respectively, fits the constraint of Lévy-walk diffusion relation Eq. (3) where α is the Lévy exponent of the solar flare waiting time series.

According to the Lévy-walk diffusion relation (3), Lévy-walk statistics yields a scaling exponent H measured by the SDA slightly larger than the scaling exponent δ measured by the DEA. The numerical results show that the difference between the scaling coefficients $H-\delta=0.05$ obtained for the temperature data sets coincides with the theoretical one obtained by using in Eq. (3) the inverse power-law exponent $\mu=2.14$ of the waiting time distribution of solar flares measured in Ref. [15]. Moreover, there is very good agreement between the exponent $\delta=0.93\pm0.02$ measured for the ocean and the exponent $\delta=0.94\pm0.02$ measured for the waiting time sequence of solar flares. As explained earlier, the significant affinity between the ocean temperature and the solar flare statistics is not unexpected due to the fact that the ocean, being very large, homogeneous, and with a high heat capacity, affords ways to respond directly to the solar activity. The land region, instead, is subject to more random fluctuations because of its inhomogeneous morphology. The difference between North and South seems to be mainly due to the different percentage of land and ocean that each hemisphere contains.

In conclusion, the results of this paper are remarkable from two points of view. The first is that the analysis confirms the efficiency of a method of analysis of time series based on the joint use of the DEA and SDA, which is the only efficient way known to us to detect Lévy statistics in the form of a Lévy walk. The second is that this analysis proves that the earth's temperature fluctuations inherit the scaling properties of the solar flare intermittency. This fact supports the hypothesis that the TSI stochastically resembles the solar flare frequency time series and that solar intermittency influences the global earth temperature also at relatively short time scales. This correspondence cannot be determined using more traditional correlation methods and it suggests that the sun is a light Lévy pulsar.

ACKNOWLEDGMENTS

N.S. thanks the Army Research Office for support under Grant No. DAAG5598D0002 and P.G. gratefully acknowledges the financial support received from the ARO through Grant DAAD No. 19-02-0037.

[1] A. S. Monin, *Weather Forecasting as a Problem in Physics* (MIT Press, Cambridge, MA, 1972).
[2] E. N. Lorenz, J. Atmos. Sci. **20**, 130 (1963).
[3] K. Lindenberg and B. J. West, J. Atmos. Sci. **41**, 3021 (1984).
[4] E. Boeker and R. van Grondelle, *Environmental Science, Physical Principles and Applications* (Wiley, Chichester, 2001).
[5] Sir Gilbert Walker, Calcutta, Indian Met. Mem. **21**, 12 (1915); **24**, 4 (1923).
[6] C. E. P. Brooks, *Climate through the Ages*, 2nd rev. ed. (Dover, New York, 1970) (original publication date 1926 and revised in 1940).
[7] C. Nicolis and G. Nicolis, Nature (London) **311**, 529 (1984).
[8] L. Gimeno, R. García, J. M. Pacheco, E. Hernández, and P. Ribera, Earth Planet. Sci. Lett. **184**, 561 (2001).
[9] J. L. Lean, J. Beer, and R. Bradly, Geophys. Res. Lett. **22**, 3195 (1995).
[10] W. Soon, S. Baliunas, E. S. Posmentier, and P. Okeke, New Astron. **4**, 563 (2000); M. Sharma, Earth Planet. Sci. Lett. **199**, 459 (2002); M. Lockwood, J. Geophys. Res., [Space Phys.] **106**, 16021 (2001); W. Soon, E. Posmentier, and S. Baliunas, Ann. Geophys. **18**, 583 (2000); N. F. Arnold, and T. R. Robinson, *ibid.* **16**, 69 (1998); S. Bravo and J. A. L. CruzAbeyro, Geophys. Res. Lett. **23**, 613 (1996); G. M. Brown and J. I. John, J. Atmos. Terr. Phys. **41**, 43 (1979); E. Friischristensen and K. Lassen, Science **254**, 698 (1991).
[11] T. Baranyi, A. Ludmany, and H. Coffey, Geophys. Res. Lett. **25**, 2269 (1998); D. Shindell, D. Rind, N. Balachandran, J. Lean, and P. Lonergan, Science **284**, 305 (1999); M. Lockwood, R. Stamper, and M. N. Wild, Nature (London) **399**, 437 (1999).
[12] E. A. Spiegel and A. Wolf, in *Chaotic Phenomena in Astrophysics*, edited by J. R. Buchler and H. Erihorn, special issue of Ann. N.Y. Acad. Sci. **497**, 55 (1987).
[13] J. D. Fix, *Astronomy, Journey to the Cosmic Frontier*, 2nd ed. (McGraw-Hill, New York, 2001).
[14] J. Polygiannakis, P. Preka-Papadema, and X. Moussas, Mon. Not. R. Astron. Soc. **343**, 725 (2003).
[15] P. Grigolini, D. Leddon, and N. Scafetta, Phys. Rev. E **65**, 046203 (2002).
[16] G. Boffetta, V. Carbone, P. Giuliani, P. Veltri, and A. Vulpiani, Phys. Rev. Lett. **83**, 4662 (1999).
[17] P. Giuliani, V. Carbone, P. Veltri, G. Boffetta, and A. Vulpiani, Physica A **280**, 75 (2000).
[18] F. Lepreti, V. Carbone, and P. Veltri, Astrophys. J. Lett. **555**, L133 (2001).
[19] M. F. Shlesinger, B. J. West, and J. Klafter, Phys. Rev. Lett. **58**, 1100 (1987).
[20] J. Klafter, M. F. Shlesinger, and G. Zumofen, Phys. Today **49** (2), 33 (1996); G. Zuomofen, J. Klafter, and M. F. Shlesinger, in *Chaos, Kinetics and Nonlinear Dynamics in Fluid and Plasmas*, Vol. 519 of *Lecture Notes in Physics* (Springer, Berlin, 1998), p. 15.

[21] N. Scafetta and P. Grigolini, Phys. Rev. E **66**, 036130 (2002).
[22] N. Scafetta, P. Hamilton, and P. Grigolini, Fractals **9**, 193 (2001).
[23] P. Allegrini, P. Grigolini, P. Hamilton, L. Palatella, and G. Raffaelli, Phys. Rev. E **65**, 041926 (2002).
[24] N. Scafetta, V. Latora, and P. Grigolini, Phys. Lett. A **299**, 565 (2002).
[25] N. Scafetta, V. Latora, and P. Grigolini, Phys. Rev. E **66**, 031906 (2002).
[26] P. Allegrini, M. Barbi, P. Grigolini, and B. J. West, Phys. Rev. E **52**, 5281 (1995).
[27] D. B. Percival and A. T. Walden, *Wavelet Methods for Time Series Analysis* (Cambridge University Press, Cambridge, England, 2000).
[28] Climate Research Unit, School of Environmental Sciences, University of East Anglia, Norwich NR4 7TJ, United Kingdom.
[29] Hadley Centre for Climate Prediction and Research, Meteorological Office, Bracknell, Berkshire, United Kingdom.
[30] P. D. Jones, T. L. Wigley, and P. B. Wright, Nature (London) **322**, 430 (1986).
[31] P. D. Jones, D. E. Parker, T. J. Osborn, and K. R. Briffa, Carbon Dioxide Information Analysis Center, Oak Ridge National Laboratory report, 2001 (unpublished).
[32] P. D. Jones, J. Clim. **7**, 1794 (1994).
[33] D. E. Parker, P. D. Jones, A. Bevan, and C. K. Folland, J. Geophys. Res., [Space Phys.] **99**, 14373 (1994).
[34] P. D. Jones, T. J. Osborn, K. R. Briffa, C. K. Folland, E. B. Horton, L. V. Alexander, D. E. Parker, and N. A. Rayner, J. Geophys. Res., [Space Phys.] **106**, 3371 (2001).
[35] N. Nicholls, G. V. Gruza, J. Jouzel, T. R. Karl, L. A. Ogallo, and D. E. Parker, in *Climate Change 1995: The IPCC Second Assessment*, edited by J. T. Houghton, L. G. Meira Filho, B. A. Callander, N. Harris, A. Kattenberg, and K. Maskell (Cambridge University Press, Cambridge, England, 1996), pp. 133–192.
[36] P. D. Jones, M. New, D. E. Parker, S. Martin, and I. G. Rigor, Rev. Geophys. **37**, 173 (1999).
[37] D. E. Parker, C. K. Folland, and M. Jackson, Clim. Change **31**, 559 (1995).
[38] C. K. Folland and D. E. Parker, Q. J. R. Meteorol. Soc. **121**, 319 (1995).
[39] N. A. Rayner, E. B. Horton, D. E. Parker, C. K. Folland, and R. B. Hackett, Climate Research Technical Note No. 74, Hadley Centre, U.K. Meteorological Office, 1996 (unpublished).
[40] http://www.cru.uea.ac.uk
[41] http://lwf.ncdc.noaa.gov
[42] W. H. Press, S. A. Teukolsky, W. T. Vetterling, and B. P. Flannery, *Numerical receipes in C* (Cambridge University Press, New York, 1997).
[43] M. B. Priestley, *Spectral Analysis and Time Series* (Academic Press, London, 1981).
[44] T. Baranyi, A. Ludmany, and H. Coffey, Geophys. Res. Lett. **25**, 2269 (1998).
[45] J. Lean, Rev. Geophys. **29**, 505 (1991).
[46] S. Mallat, *A Wavelet Tour of Signal Processing* (Academic Press, London, 1998).
[47] N. Scafetta, T. Imholt, P. Grigolini, and J. Roberts, physics/0202012.
[48] B. B. Mandelbrot, *The Fractal Geometry of Nature* (Freeman, New York, 1983).
[49] P. Grigolini, L. Palatella, and G. Raffaelli, Fractals **9**, 439 (2001).
[50] H. E. Stanley, L. A. N. Amaral, P. Gopikrishnan, P. Ch. Ivanov, T. H. Keitt, and V. Plerou, Physica A **281**, 60 (2000).
[51] C.-K. Peng, S. V. Buldyrev, S. Havlin, M. Simons, H. E. Stanley, and A. L. Goldberger, Phys. Rev. E **49**, 1685 (1994).
[52] B. V. Gnedenko and A. N. Kolomogorov, *Limit Distributions for Sums of Random Variables* (Addison-Wesley, Reading, MA, 1954).
[53] W. Feller, Trans. Am. Math. Soc. **67**, 98 (1949).
[54] G. Tréfan, E. Floriani, B. J. West, and P. Grigolini, Phys. Rev. E **50**, 2564 (1994).
[55] P. Allegrini, P. Grigolini, and B. J. West, Phys. Rev. E **54**, 4760 (1996).
[56] N. Scafetta and B. J. West, Phys. Rev. Lett. **90**, 248701 (2003).
[57] S. Corti, F. Molteni, and T. N. Palmer, Nature (London) **398**, 799 (1999).
[58] R. C. Willson and A. V. Mordvinov, Geophys. Res. Lett. **30**, 1199 (2003).
[59] D. V. Hoyt and K. H. Schatten, *The Role of the Sun in the Climate Change* (Oxford University Press, New York, 1997).